nature photonics

Review article

https://doi.org/10.1038/s41566-023-01299-6

Label-free biomedical optical imaging

Received: 27 February 2023

Accepted: 22 August 2023

Published online: 16 November 2023

Check for updates

Natan T. Shaked [1] ✉, Stephen A. Boppart [2], Lihong V. Wang [3] & Jürgen Popp [4,5]

Label-free optical imaging employs natural and non-destructive approaches to visualize biomedical samples for both biological assays and clinical diagnosis. At present, this field revolves around multiple technology-oriented communities, each with a specific focus on a particular modality, despite the existence of shared challenges and applications. As a result, biologists or clinical researchers who require label-free imaging are often not aware of the most appropriate modality to use. This Review presents a comprehensive overview of, and comparison among, different label-free imaging modalities and discusses common challenges and applications. We expect this Review to facilitate collaborative interactions between imaging communities, push the field forwards and foster technological advancements and biophysical discoveries, as well as facilitate new avenues in clinical detection, diagnosis and monitoring of diseases.

Biomedical optical imaging refers to multi-point measurement techniques that use light to capture images of biological samples in vitro or in vivo. Many biomedical samples, however, do not induce sufficient imaging contrast and important biological details might be missed in the resulting images. For example, some biological samples, such as cells in vitro, are optically semi-transparent and induce minimal light absorption, which is one of the primary sources of contrast in conventional optical imaging. Exogenous labelling agents, such as fluorophores or specific stains with chemical properties that allow binding to specific components in the biological samples, are widely used to induce the missing imaging contrast. Alternatively, it is possible to genetically modify the cells, organisms or the resulting samples to express fluorescence or other useful optical properties. These techniques are typically used in animal studies, or in vitro diagnosis, when the sample is disposed of shortly after imaging it. Any form of exogenous labelling or genetic modifications perturbs the natural biological processes, dynamics and response of live cells or tissues, degrades the vitality of the sample and might be fatal in longer-term longitudinal studies. Moreover, the use of exogenous labelling often has confounding factors such as off-target binding, non-specific binding or incomplete binding, making quantification and reproducibility a challenge. These are some of the common reasons why label-based imaging techniques are not recommended for use during in vivo imaging for medical diagnosis and therapy, especially in human participants. Furthermore, label-based imaging techniques are problematic even for use during in vitro imaging of live human cells when the sample is needed for further medical treatments, such as when imaging stem cells for personalized medicine or gamete cells during in vitro fertilization. In all these clinical settings, label-free imaging would be preferred as it does not require expensive and time-consuming approvals for the chemical marker use as a drug.

Label-free optical imaging captures the intrinsic properties of the sample, such as the sample's refractive index variations, autofluorescence, molecular vibrations, birefringence, scattering or absorption properties, to generate imaging contrast. These techniques are non-perturbative to the measurement and the following analysis, provided that the optical energy needed is not too high to damage the structure, function, molecular composition or physiology of the cells or tissues

[1]Department of Biomedical Engineering, Faculty of Engineering, Tel Aviv University, Tel Aviv, Israel. [2]Beckman Institute for Advanced Science and Technology, Department of Electrical and Computer Engineering, Department of Bioengineering, University of Illinois Urbana-Champaign, Urbana, IL, USA. [3]Caltech Optical Imaging Laboratory, Andrew and Peggy Cherng Department of Medical Engineering, Department of Electrical Engineering, California Institute of Technology, Pasadena, CA, USA. [4]Leibniz Institute of Photonic Technology, Member of Leibniz Health Technologies, Member of the Leibniz Centre for Photonics in Infection Research, Jena, Germany. [5]Institute of Physical Chemistry and Abbe Center of Photonics, Friedrich Schiller University Jena, Jena, Germany. ✉e-mail: nshaked@tau.ac.il

https://doi.org/10.1038/s41566-023-01299-6

Table 1 | Summary of key performance characteristics of major label-free biomedical imaging approaches

Method	Spatial resolution	Imaging depth	Speed	Main source of contrast	Main applications	System complexity and cost	Can it be used in vivo?	Is it clinically widely available?
PhM	Submicrometre	Tens of micrometres	****	Refractive index	Cell structure	*	No	Yes
Polarization microscopy	Submicrometre	Tens of micrometres	****	Birefringence	Cell and tissue structure (membranes and filament arrays, for example, collagen fibres; cell spindle)	*	Yes (together with other methods)	Yes
OCT	Several micrometres	Several millimetres	****	Refractive index, speckle/phase variance, Doppler, strain and shear stress	Tissue structure; blood circulation; biomechanics	**	Yes	Yes
Harmonic generation microscopy	Submicrometre	Submillimetre	***	High-order nonlinear susceptibility	Cell and tissue structure SHG:non-centrosymmetric structures and fibrillar structures, such as collagen or elastin in connective tissues, or myosin and microtubules in muscle fibres THG: interfaces and optical heterogeneities, such as lipid-based biological membranes	****	Yes	No
Autofluorescence microscopy	Submicrometre	Submillimetre	***	Endogenous fluorochromes	Cell and tissue structure, NAD(P)H, FAD, keratin and elastin; redox; metabolic dynamics	***	Yes	No
IR-absorption microscopy	Several micrometres	Submillimetre	****	Absorption	Endogenous tissue chromophores (haemoglobin, melanin, water and collagen)	**	Yes	No
Raman microscopy	Submicrometre	Submillimetre	* (linear) *** (nonlinear)	Raman scattering of molecular vibrations	Selective macromolecular vibrations of lipids, proteins, DNA and so on	** (linear) **** (nonlinear)	Yes	No
PAT	Scalable: submicrometre to tens of micrometres	Scalable: submillimetre to tens of millimetres	****	Absorption	Cell and tissue structure; vasculature	****	Yes	No

Asterisks are for qualitatively comparing speed and complexity and cost between methods. ****More than 10 megavoxels^{-1} in reasonable, clinically attainable resources (speed column). Details refer to the common version of each method.

being measured. The optical set-up needs to be adjusted according to the intrinsic source of the imaging contrast mechanism in each label-free imaging technique. A few label-free imaging techniques, such as Zernike's phase contrast of in vitro cells, are relatively simple to implement and use, and therefore are widely available to biologists and clinicians. Most label-free imaging techniques, however, require more complex and expensive optical set-ups. For example, if the source of contrast is Raman scattering, one would need to carefully design the illumination wavelength and intensity of the excitation source and use an imaging spectrograph to obtain the sample image. This higher degree of system complexity causes some label-free techniques to be intriguing and inaccessible to biologists and clinical researchers, leaving the field of label-free imaging to be centralized around several technology-oriented communities, each of which is leading in one or a few label-free techniques, while missing important biomedical applications being pursued in other label-free imaging communities.

This Review attempts to make label-free imaging accessible to cross-community investigators and users by first discussing the working principles and special considerations for selecting the most suitable label-free imaging modality for a given application, then the future challenges of the field and leading biomedical applications.

Comparative analysis

The development and use of label-free imaging can be categorized into cases where labelling is not allowed and cases where labelling is allowed but label-free imaging provides better performance. The first type of cases might occur where the sample needs to be used for treatment after imaging it, for immunotherapy drug testing, for regenerative medicine (where specific labelling agents do not yet exist), for toxicity measurements, for in vivo applications or for clinical applications where point-of-procedure or point-of-care detection, diagnosis or guidance is needed (for example, intraoperative diagnosis such as optical biopsy and intra-vital microscopy). The second type of cases is where labelling is allowed, but still label-free imaging provides better measurements, such as more quantitative and infomative data layers.

A comparison between various label-free imaging techniques is presented in Table 1. The key criterion that should be considered when choosing a label-free imaging technique per application is the intrinsic contrast mechanism, alongside the physics of the chosen technique, and its presence in the sample measured. For example, a cell's integral refractive index, which can be measured via interference-based phase microscopy (PhM)[1–6] (Fig. 1a–d), is proportional to the cell dry mass surface density[4]. This parameter cannot be measured via label-based imaging techniques, in which the labelling agent can indicate the location of the labelled organelle but the greyscale value of each point in the image cannot typically be interpreted quantitatively. To obtain a three-dimensional (3D) image of an individual cell, with sectioning, interferometric computed tomography[7,8] can be used, where quantitative PhM is performed from multiple angles to generate 3D cellular refractive index maps with a resolution of less than half a micrometre (Fig. 1e,g)[9].

Polarization microscopy is typically used to analyse optical anisotropy due to molecular order, where the average molecular orientation is not random. This may occur in biological samples containing extensive membranes, such as photoreceptors on the retina, or in biological samples containing filament arrays, such as collagen fibres[10] and cell mitotic spindles[11]. Birefringence, anisotropy of the refractive index, can be observed in sperm cells and oocytes[12].

https://doi.org/10.1038/s41566-023-01299-6

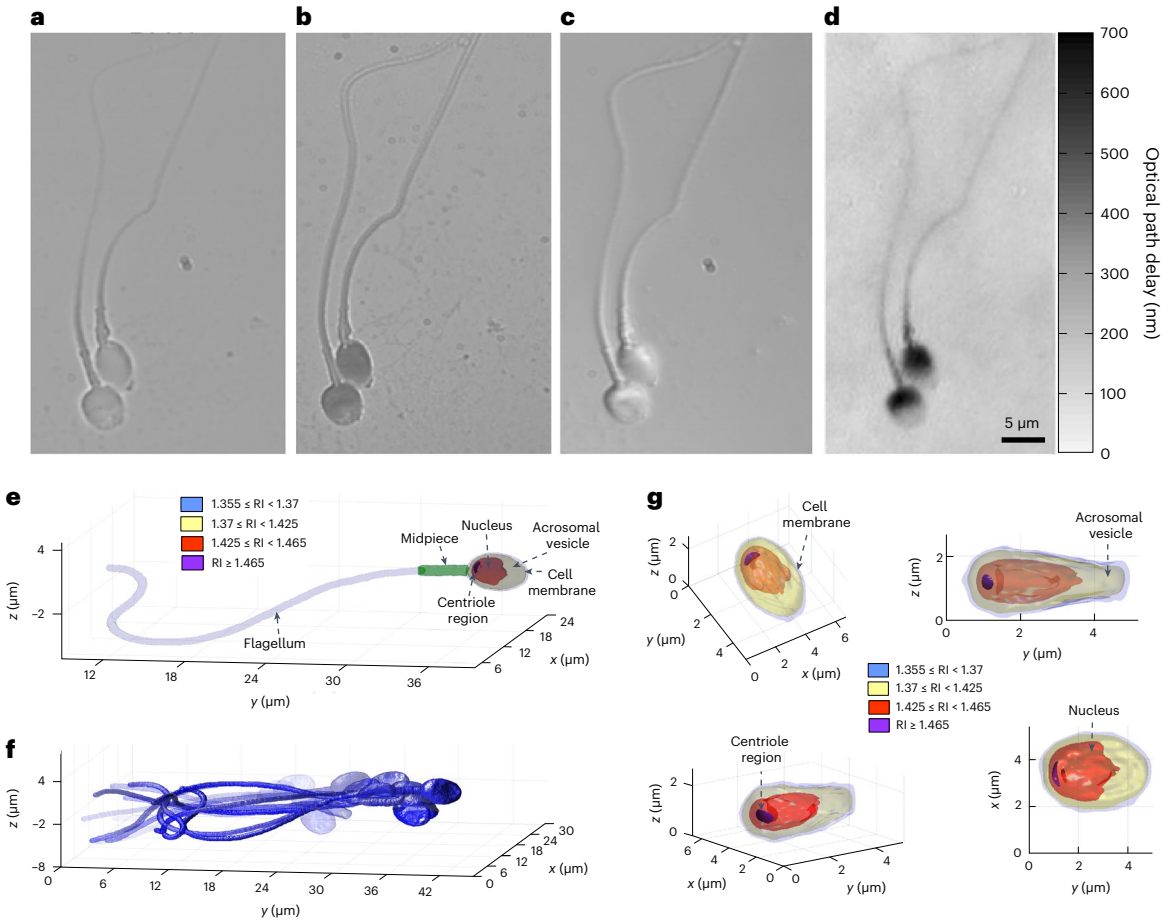

Fig. 1 | Comparison of imaging methods of human sperm cells. a, Label-free bright-field imaging, presenting low contrast where the inner content of the cell cannot be seen. **b**, Label-based bright-field imaging (not permitted in human in vitro fertilization). **c**, Label-free differential interference contrast (DIC) microscopy, a qualitative PhM method. **d**, Label-free quantitative PhM (ref. 6). **e**,**f**, High-resolution label-free dynamic 3D imaging of a sperm cell swimming freely, acquired by interferometric computed tomography. RI, refractive index. **e**, A single frame from the 3D motion, revealing the internal structure of the sperm cell. **f**, Overlay of 15 frames from the 3D motion. **g**, The sperm cell head 3D refractive index profile from various viewpoints. Panels reproduced with permission from: **e**,**g**, ref. 9 under a Creative Commons licence CC BY 4.0. Panel **f** adapted with permission from ref. 9 under a Creative Commons licence CC BY 4.0.

Optical coherence tomography (OCT)[13–15] uses light interference from a partially coherent light to obtain contrast from the tissue refractive index changes, offering the capability of optical sectioning and thus 3D imaging of multi-layer tissues ex vivo or in vivo with a spatial resolution on the micrometre scale and a depth of penetration in most tissues on the scale of 1–2 mm. Various clinical applications of OCT, including ophthalmic imaging[15–17], coronary artery disease detection[18,19], intraoperative optical biopsy in cancer detection[20–22], endoscopic evaluation of the gastrointestinal tract[23,24], skin imaging in dermatology[25–27] and blood flow imaging in vivo[28,29], are shown in Fig. 2. Furthermore, phase-variance OCT can sensitively detect movement, such as in dynamic cells[30] or the retinal microvasculature[31,32].

Harmonic generation microscopy creates imaging contrast based on the high-order nonlinear susceptibility of the sample. Second-harmonic generation (SHG) occurs at non-centrosymmetric molecular structures or interfaces and most commonly from fibrillar structures (such as collagen or elastin in connective tissues) changing dramatically during carcinogenesis, or myosin and microtubules in muscle fibres and metastatic tumour cells[33–35]. Third-harmonic generation (THG) occurs at interfaces across which there is a large change in the refractive index, such as across a lipid-based biological membrane and the surrounding aqueous microenvironment[36,37]. Autofluorescence microscopy is based on measuring the fluorescence from endogenous biomolecules, including nicotinamide adenine dinucleotide phosphate (NAD(P)H), flavin adenine dinucleotide (FAD), tryptophan and others. Specifically, NAD(P)H and FAD images indicate the metabolic activity of cells and tissues. Optical excitation of these biomolecules can occur through single-photon interactions, but multiphoton interactions in two-photon autofluorescence (2PF), three-photon autofluorescence (3PF) or higher multiphoton autofluorescence offer advantages of higher spatial resolution, higher signal-to-noise ratios, deeper imaging penetration with incident wavelengths close to infrared (IR) and optical sectioning capabilities[38]. Simultaneous label-free autofluorescence multi-harmonic microscopy (SLAM)[39] combines 2PF, 3PF, SHG and THG (Fig. 3). Multiple investigators have used the intensity values of this autofluorescence to calculate redox ratios and to characterize the metabolic properties of cells in vitro, living tissues in vivo or fresh tissue specimens[40,41]. Clearly such dynamic metabolic properties cannot be fully characterized in chemically processed, fixed and stained sections, and the use of exogenous dyes or stains would affect the inherent metabolic processes being measured. Time-correlated single-photon counting[42] and, more recently, fast direct sampling techniques[43] can capture the fluorescence lifetime, or the decay time of the fluorescence emission, in fluorescence lifetime imaging microscopy (FLIM). The decay profile offers another label-free contrast parameter that is sensitive to many of the microenvironmental conditions surrounding

the autofluorescent molecules, such as chemical composition and pH, as well as any perturbation to these conditions[44].

Label-free hyperspectral imaging is able to capture the contiguous spectrum for each pixel in the image over a selected wavelength bandwidth to detect physiological changes via their absorption, reflectance or scattering spectral signatures, with limited molecular specificity. Hyperspectral imaging can detect endogenous tissue chromophores such as haemoglobin, melanin, water and collagen contents[45]. Specifically, in IR-absorption microscopy, characteristic molecular vibrations of cell and tissue constituents are excited by the absorption of radiation with wavelengths between 2.5 and 50 μm (4,000–200 cm^{-1}). The introduction of tunable quantum-cascade lasers has made IR excitation with a high photon density possible, partially compensating for the appearance of strong IR water absorption bands in the IR spectra of biomedical samples that mask other relevant bands[46–48]. Photothermal IR microscopy is based on the non-radiative transformation of absorbed energy into heat, allowing submicrometre spatial resolution. Using mid-IR illumination, the absorbed heat leads to local expansion and changes in the refractive index of the sample, which can be detected in the visible range and yield better lateral resolution than classic IR spectroscopy[49,50].

Raman microscopy is based on the detection of inelastic Raman scattering via molecular vibrations that are specific to chemical bonds inside the molecule—that is, lipids, carbohydrates, pigments, DNA, RNA, proteins and so on[51–54]. Linear (spontaneous) Raman spectroscopy is characterized by intrinsically small scattering cross-sections, which makes it challenging to acquire hyperspectral Raman images of large tissue areas. This disadvantage can be overcome by using nonlinear coherent Raman scattering, including coherent anti-Stokes Raman scattering (CARS)[55] (Fig. 4, as combined with SLAM[56,57]) and stimulated Raman scattering[58,59]. These techniques enhance the intrinsically weak Raman signal and avoid the appearance of a large autofluorescence background, but have reduced molecular selectivity because they can image only one or a few characteristic Raman bands.

Photoacoustic tomography (PAT)[60] provides 3D imaging based on the photoacoustic effect. When light is absorbed by molecules and converted to heat, an acoustic wave is generated due to thermoelastic expansion. The acoustic wave is detected with negligible scattering to form a high-resolution tomographic image. Consequently, PAT combines the optical contrast of molecular absorption and ultrasonic resolution despite optical diffusion, providing multiscale high-resolution structural and functional imaging[61–63] in vivo at depths beyond the optical diffusion limit (~1 mm in human skin). In focused scanning PAT[64], the acoustic focusing of an ultrasonic transducer or the optical focusing of an objective lens provides lateral resolution, whereas the acoustic time of flight offers axial resolution. In photoacoustic computed tomography, usually hundreds to thousands of unfocused ultrasonic transducers receive photoacoustic waves in parallel. An inverse reconstruction algorithm[65] is used to reconstruct a tomographic image. The first mode costs less, but the second mode provides greater speed and more uniform spatial resolution. PAT is capable of in vivo[61,66–69] and in vitro[70] imaging at multiple length scales, ranging from subcellular organelles to human organs or small-animal organisms[71] with the same contrast origin, as shown in Fig. 5.

After determining whether a certain intrinsic property exists in the sample, which will lead to the selection of the appropriate label-free imaging method as reviewed above, other key parameters should be considered. As shown in Table 1, these include the target imaging depth, spatial resolution and acquisition time. The selection of these parameters requires knowledge of the physics of the optical system and the contrast mechanism. As a rule of thumb, there is a trade-off between obtaining a high resolution and a large imaging depth. For example, PAT offers a variable trade-off between imaging depth and spatial resolution due to the ultrasonic physics. The ultrasonic attenuation coefficient is approximately proportional to the ultrasonic frequency, while the ultrasonic spatial resolution in length is inversely proportional to the ultrasonic frequency. Within the reach of diffuse light in biological tissues, the ratio of the imaging depth to the spatial resolution is approximately constant on the order of 200, resulting in the dashed line shown in Fig. 5g. As another example, the lateral resolution limit in time-domain OCT is proportional to the wavelength of the light source divided by the numerical aperture of the imaging system, whereas the depth of focus (imaging depth range) is proportional to the wavelength of the light source divided by the square of the numerical aperture of the imaging system; thus, achieving a smaller resolution limit comes at the cost of decreasing the depth of focus. The axial resolution in time-domain OCT, on the other hand, is proportional to the square of the central wavelength of the light source divided by its wavelength bandwidth. Thus, increasing the central wavelength will damage both the lateral and axial resolutions, but will increase the imaging depth range.

Exogenous fluorescence labelling agents tend to photobleach under high excitation powers, resulting in a variable and often unpredictable time-dependent loss of imaging contrast. When rapid imaging is needed, the number of fluorescence photons might be too small to be detected, resulting in low single-to-noise ratios. Thus, label-free imaging can be beneficial for imaging very rapid dynamic phenomena where fluorescence imaging fails. Depending on the speed of the dynamics, one might prefer label-free imaging techniques that do not require sample scanning, such as PhM, polarization microscopy, FLIM or optical parametrically gated microscopy[72].

Of course, the system construction and use complexity, as well as its overall cost, are additional considerations. Nonlinear label-free imaging techniques, such as harmonic generation microscopy, Coherent Raman microscopy and so on, typically require the use of ultrashort (femtosecond or picosecond) optical pulses with a sufficient peak power to induce nonlinear effects in biological samples, which are generally weak and require more complex imaging systems. The recent development of turn-key high-intensity ultrashort lasers in label-free imaging resulted in a large improvement in the penetration depth, optical resolution and acquisition speed. For example, simultaneous absorption of two or three photons leads to high localization of the autofluorescent light (2PF and 3PF, respectively) or the high harmonic generation signal, as such nonlinear absorption processes can only take place in an extremely small volume.

Multiphoton imaging using near-IR femtosecond lasers is also characterized by high penetration depths. However, nonlinear imaging approaches might require higher illumination intensity. Attention must be paid to maximizing the optical power to generate a larger

Fig. 2 | Label-free OCT applications. a, Ophthalmic OCT of the human retina (cross-section) delineating individual retina layers. Scale bars, 200 μm **b**, Computational adaptive optics to correct optical aberrations in the human eye to enable en face OCT of individual photoreceptors in the mosaic. RNFL, retinal nerve fibre layer; GCL/IPL, ganglion cell layer/inner plexiform layer; INL, inner nuclear layer; OPL, outer plexiform layer; ONL, outer nuclear layer; IS/OS, inner segment/outer segment; RPE, retinal pigment epithelium. **c**, Fibre-optic catheter-based radial OCT of the human coronary artery to assess stent apposition compared with intravascular ultrasound (greyscale image). **d**, Intraoperative OCT for surgical oncology guidance. 3D images of human lymph nodes reveal increased scattering following metastatic involvement. Scale bars, 500 μm. **e**, OCT of human skin, revealing architectural differences as a result of atopic dermatitis. **f**, 3D OCT of mouse embryonic development, with real-time functional assessment of cardiac dynamics. Panels reproduced with permission from: **b**, ref. 17, Springer Nature Limited; **c**, ref. 19, British Medical Association; **d**, ref. 21 under a Creative Commons license CC BY 4.0; **f**, ref. 29, Optica. Panel **e** adapted with permission from ref. 27, Optica.

https://doi.org/10.1038/s41566-023-01299-6

signal, while minimizing it to avoid damage to the cells and tissues due to photothermal or photomechanical effects. The interplay of several factors should be considered in the optical power optimization. These include the pulse energy, which relates to the laser repetition rate for a given optical power; the pixel dwell time, which relates to the scanning speed; the illumination wavelengths, where the IR regime close to the visible is preferable over the visible regime due to lower photon absorption; and the illumination pattern, which relates to the laser

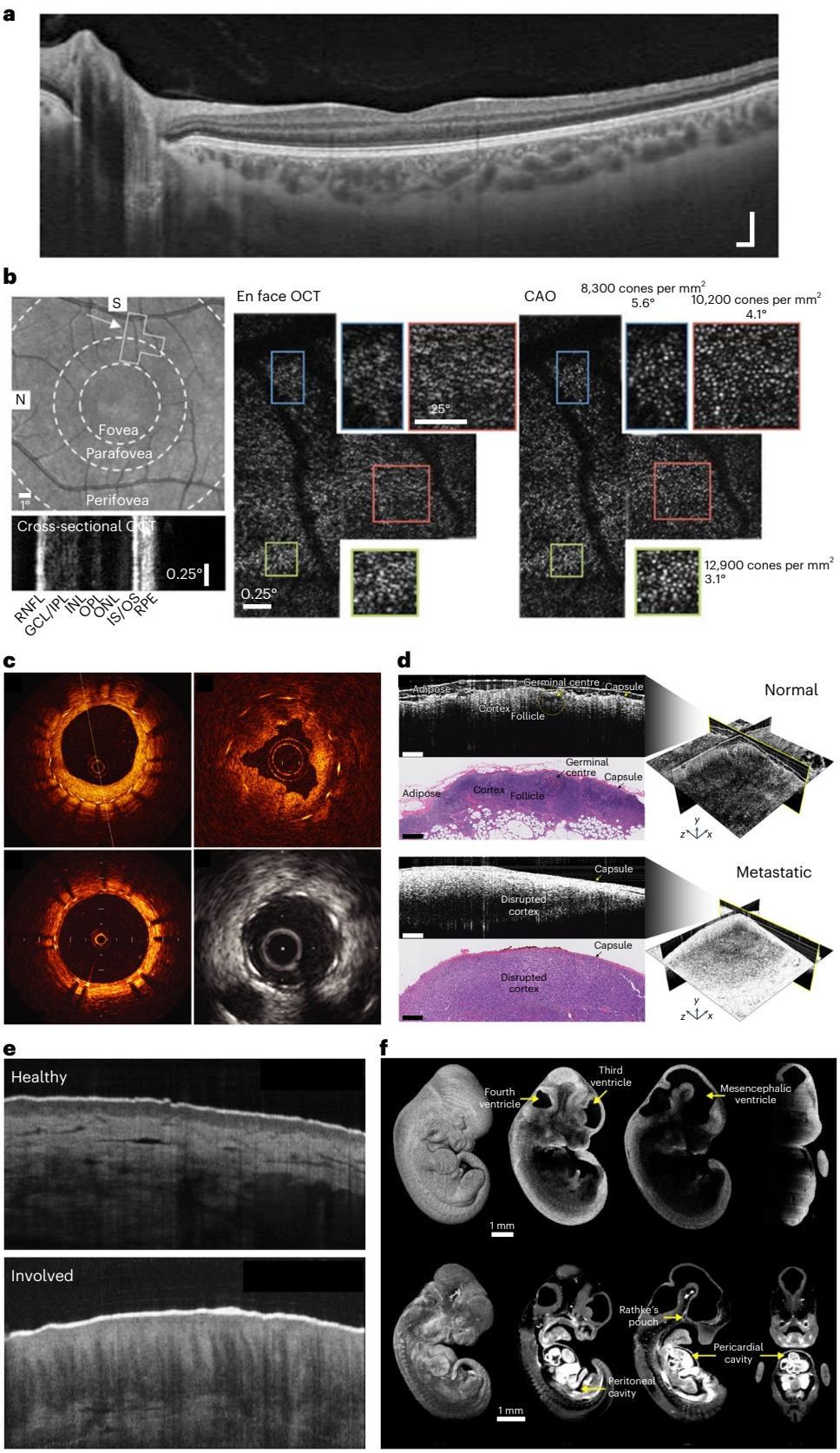

https://doi.org/10.1038/s41566-023-01299-6

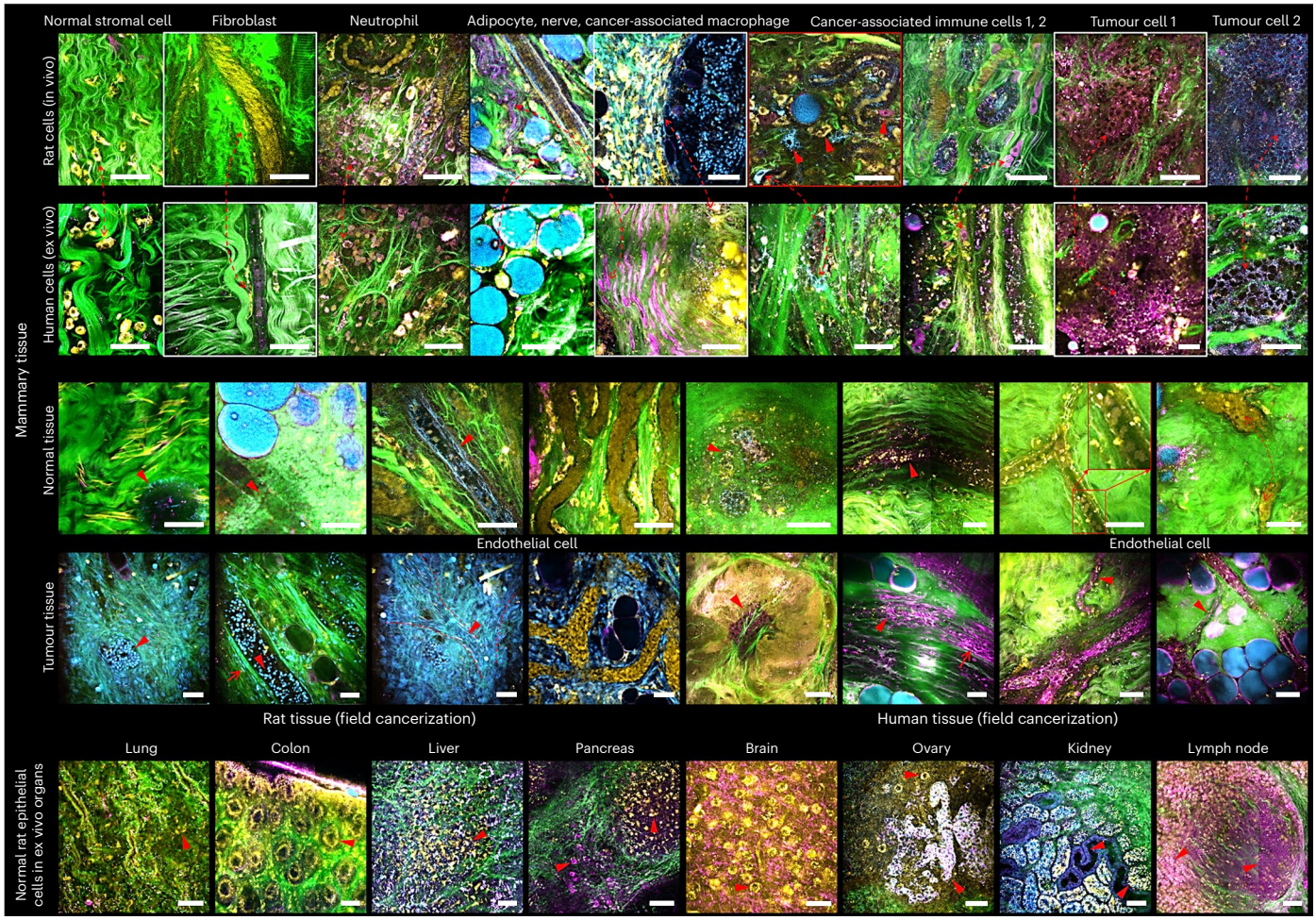

Fig. 3 | Image atlas obtained by SLAM. Images of various normal and cancer tissues from fresh, unstained human and rat biopsy specimens, in vivo and ex vivo, showing various endogenous contrast channels. Yellow, 2PF of FAD, blue, 3PF of NAD(P)H; green, SHG of fibrous structures (collagen); magenta, THG of lipid–aqueous interfaces. Other colours are a result of the relative colour mixing between the overlaid channels. The red arrowheads point to particular cells and structures of interest. The dashed red lines with arrowheads draw correlations between features of the cells found in both the rat and the human tissues. Scale bars, 25 µm.

irradiance per sample space and the exposure times per sample position. This trade-off can be managed by utilizing increasingly sensitive optical detectors and optical signal amplification to detect the weak harmonic generation signals for imaging[72].

Future challenges

Label-free imaging utilizes endogenous intrinsic signals, rather than specific exogenous markers, while displaying both morphology and chemical composition and presenting no confounding factors associated with targeting, no biochemical perturbations and no potential toxicity. It thus allows rapid clinical translation, without drug approvals, as well as imaging of fresh tissues, even in vivo. In addition, it allows new forms of contrast to be recorded and new features to be extracted that cannot be obtained when using exogenous markers, and thus it can provide high dimensionality for AI analysis. Specifically, label-free imaging can provide structural, functional and metabolic imaging, especially with highly multiplexed and multimodal imaging that is based on multiple contrast mechanisms and physics. Despite these great advantages, the main disadvantage of label-free imaging is limited sources of endogenous contrast. For some of the methods, this might result in lower molecular specificity and weak signals with less clear origins. For these methods, optical energy deposition may occur when using higher incident energy/power while attempting to compensate for the weaker signals. Furthermore, for exogenous labelling, and in most cases, the same hardware system can be used to image various biological molecules. The burden of system complexity is then shifted to chemistry. In contrast, each label-free imaging method, typically requires a specific hardware system that must be tuned to image various molecules, prompting the development of multimodal imaging systems. Accordingly, the challenges in the field of label-free imaging and possible future solutions are discussed below.

Some internal contrast mechanisms used in label-free imaging are not specific to certain cell organelles, receptors on cell membranes or biomolecules. For these techniques, obtaining label-free specificity is a great challenge. For example, the refractive index of the cell nucleus might be close to (or even lower than) that of the cell cytoplasm[73]. It is therefore difficult to determine the boundaries of the nucleus via refractive index-based label-free imaging techniques, whereas this is a relatively simple task when exogenous labelling agents are used. Recent AI-based approaches have enabled virtual tissue and cell staining[74–77], also referred to as computational staining or virtual histology. In this case, a deep neural network is trained on label-free and label-based images, so that after training, the network can take a label-free image of the same type used for training and make it look as if the sample has been chemically labelled. These techniques have been shown to be useful for virtual histopathology of tissue slices and individual cells

https://doi.org/10.1038/s41566-023-01299-6

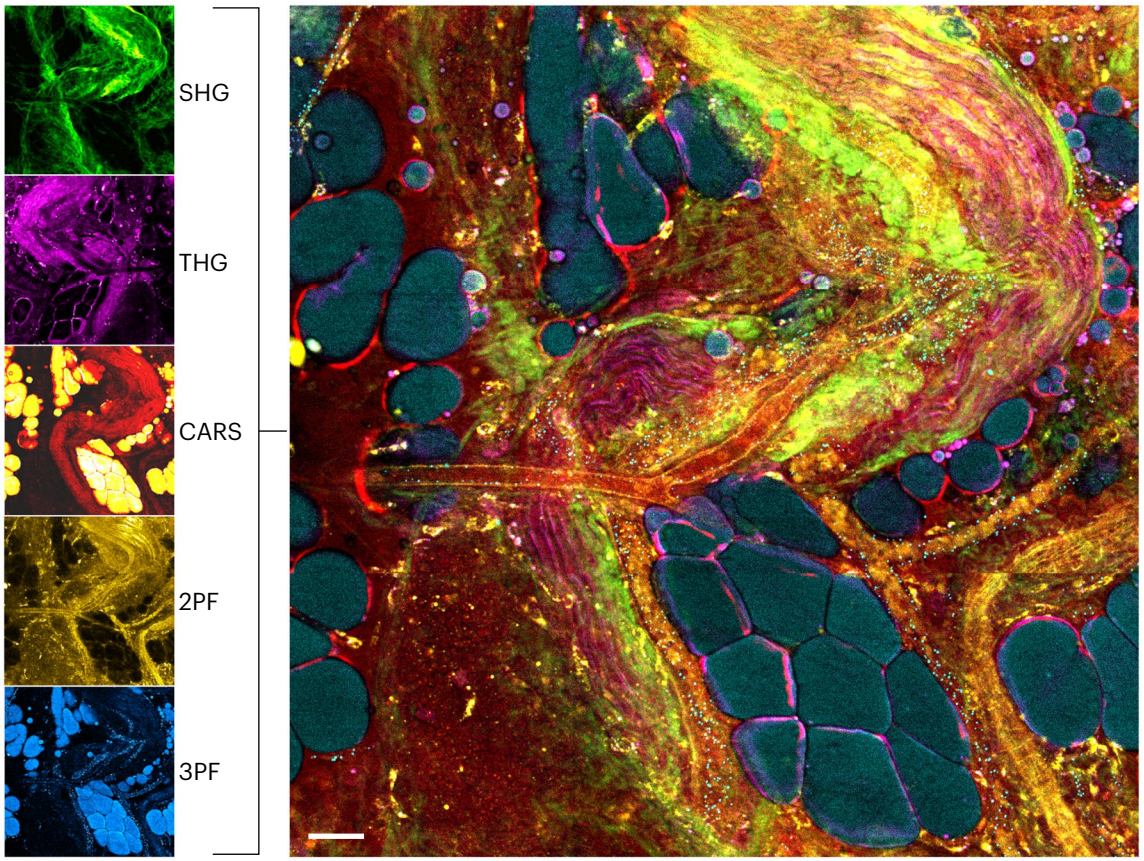

Fig. 4 | Single-shot label-free multimodal nonlinear imaging. Using a single fibre-laser pumped photonic crystal fibre source to generate supercontinuum illumination, along with parallel multi-channel photomultiplier tube detectors, multiple nonlinear processes can be excited in tissue simultaneously and detected to generate a spatially and temporally co-registered label-free image of tissue microstructure, molecular composition, function and metabolism (SHG, THG, CARS, 2PF and 3PF). Multimodal images, radar plots and spectra for normal and tumour tissues can be found in ref. 57. Scale bar, 50 µm. Figure adapted with permission from ref. 56, AAAS.

in vitro, avoiding standardization problems that might occur when using chemical staining, as well as providing virtually stained images when chemical cell staining is not permitted, such as during in vitro fertilization[75]. These AI-based methods work as long as the label-free images can sufficiently define, in a collective manner, the basis for training the deep network, even if at the single-image level, virtual staining cannot be done at first sight. AI can also help in identifying the source of a label-free signal, or even discern between several sources of signals when multimodal label-free imaging is implemented. Specifically, automated interpretation of label-free hyperspectral datasets with AI instead of the naked eye offers new possibilities in the derivation of secondary data and conclusions from the primary information[78]. We believe that in the near future, with increasing computational processing power and fast acquisition and imaging techniques, these AI-based techniques will be more widely used to apply in vivo virtual staining as well[79,80]. Furthermore, intensive cross-disciplinary collaborations between photonics and AI experts is expected to enable new technological concepts in the field of label-free imaging, allowing new hardware-based AI-integrated systems to be developed.

Obtaining label-free nanoscopy, meaning imaging of nanoscale objects without exogenous chemical labelling, is another challenge yet to be addressed. Far-field optical microscopy is typically restricted by the diffraction of light to approximately 200–500 nm. So far, the main advances have been achieved with super-resolved fluorescence microscopy, such as photoactivated localization microscopy (PALM)[81], which received the 2014 Nobel Prize in Chemistry, and stochastic optical reconstruction microscopy (STROM). These techniques enable label-based nanoscopy of biological cells utilizing specific nanoscale fluorescence emitters. On the other hand, overcoming the far-field diffraction limit without cell labelling is extremely challenging due to the low number of photons originating from unlabelled nanoscale objects, especially when performing rapid 3D imaging. Preliminary label-free super-resolution results have been demonstrated for quantitative phase imaging[82] and Raman spectroscopy[83,84], as well as using photoacoustic[85] and photothermal[86] effects. Another potential approach to obtain label-free nanoscopy is the label-free localization of nanoparticles. Specifically, interferometric scattering microscopy[87] allows label-free localization of nanoparticles as small as 5 nm, including viruses and proteins, by recording their scattering signals. Mass photometry has been used together with interferometric scattering microscopy to record specific protein assembly and disassembly[88,89]. As the size of the nanoparticles detected decreases, the signal-to-noise ratio decreases exponentially, requiring extremely sensitive detectors to allow full-field imaging. Finding stochastic or switchable mechanisms of the scatterers, similarly to fluorophores in PALM and STORM, which can be activated naturally during label-free imaging, might transform label-free localization techniques into label-free nanoscopy techniques. Of course, future approaches might also utilize a combination of experimental label-free optical techniques with computational optics or AI-based methods.

Another challenge is in vivo label-free imaging. Being able to ignore a patient's natural dynamics, such as respiratory or cardiac motion, is a challenge of any in vivo imaging technique. While some label-free imaging techniques, such as OCT and PAT, are regularly used for in vivo imaging, other techniques, such as PhM, are more challenging to implement in vivo mainly due to the low rates of photon generation and

https://doi.org/10.1038/s41566-023-01299-6

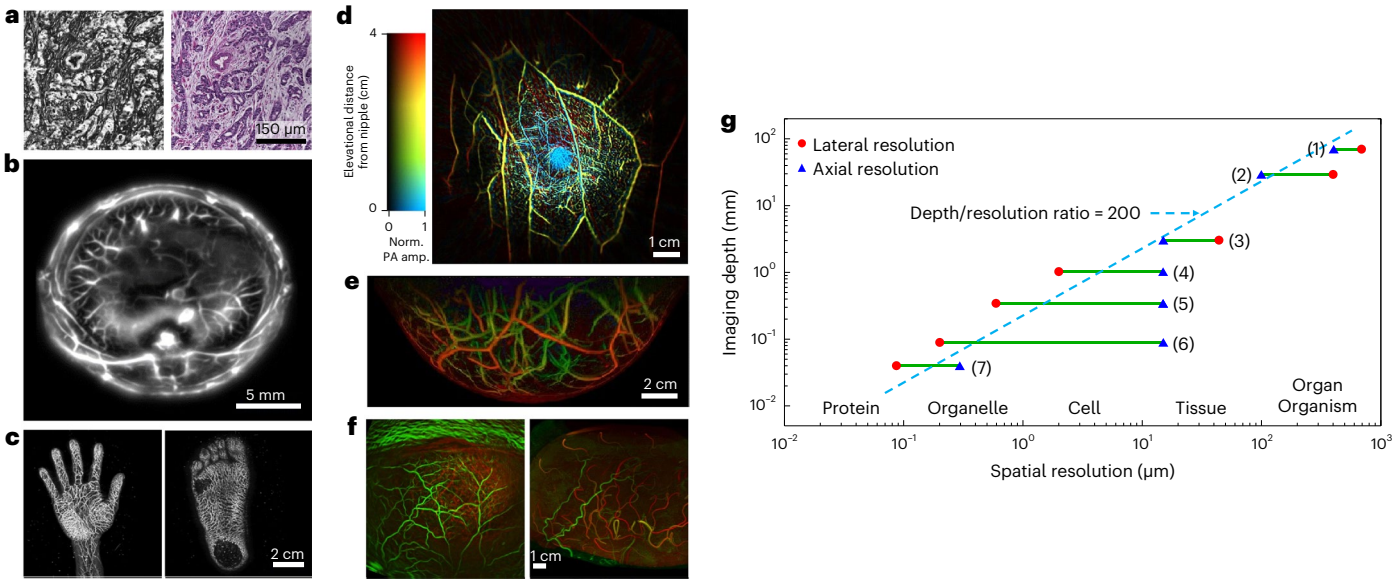

Fig. 5 | Multiscale label-free photoacoustic imaging of molecular absorption. **a**, Photoacoustic pathology. Left: photoacoustic microscopic image of a breast cancer specimen without staining. Right: conventional histologic image of the same breast cancer specimen with haematoxylin and eosin staining. **b**, In vivo whole-body photoacoustic image of a rodent acquired in a full-ring detection geometry. **c**, In vivo 3D photoacoustic images of a human hand (left) and foot (right). **d**, Single-breath-hold photoacoustic image of the breast acquired in a full-ring detection geometry. Norm., normalized; PA amp., photoacoustic amplitude. **e**, Photoacoustic image of the breast acquired in a hemispherical detection geometry. **f**, Functional photoacoustic image of the human brain acquired in hemispherical detection geometry (left) versus functional MRI image (right). **g**, Graph illustrating the scalability of photoacoustic imaging. The ranges indicated on the graph are: (1) low-frequency photoacoustic tomography; (2) photoacoustic macroscopy; (3) acoustic-resolution photoacoustic microscopy; (4) optical-resolution photoacoustic microscopy; (5) submicrometre photoacoustic microscopy; (6) sub-wavelength photoacoustic microscopy; (7) super-resolution photoacoustic microscopy. Panels reproduced with permission from: **a**, ref. 70, AAAS; **b**, ref. 71, Springer Nature Limited; **c**, ref. 66 under a Creative Commons license CC BY 4.0; **d**, ref. 67 under a Creative Commons license CC BY 4.0; **f**, ref. 69 under a Creative Commons license CC BY 4.0. Panel **e** courtesy of the authors of ref. 68.

collection, and the scattering properties of tissues, which yield noisy images that are hard to interpret, as well as the fact that some of these techniques are typically implemented in transmission mode, rather than in reflection mode. Fibre-based label-free imaging via various catheters, endoscopes and needle probes has enabled techniques with limited imaging penetration depths of several millimetres in internal organs. These techniques are relevant for deep in vivo imaging, utilizing portable imaging systems in clinical environments such as the operating room[90,91]. Specifically, to avoid ex vivo examination of fixed and stained tissue samples by a pathologist, in vivo endoscopy can be performed. New approaches are needed for reliable intraoperative tissue diagnosis when time-consuming procedures cannot be used, with a clear preference for label-free imaging approaches. As another example, clinically usable Raman fibre probes in combination with field-deployable compact Raman microscopes and endoscopes have been used for the intraoperative detection of tumours[54,92]. Still, future innovations are needed in the beam-delivery devices, such as hand-held probes, fibre-optic based catheters and endoscopes, and needle-based probes, which will permit high-resolution label-free nonlinear optical imaging at deeper sites within the human body. The implementation of such a nonlinear multimodal imaging approach for in vivo tissue screening requires new endo-spectroscopic probe concepts, which is a major technological challenge[93].

On-chip implementations might reduce the complexity of the optical systems and make label-free imaging techniques more attainable for direct clinical in vivo or in vitro uses. For example, photonic integrated waveguide gratings were recently used for on-chip OCT[94], and nanophotonic waveguides were used to excite and collect signals in the close vicinity of a waveguide for on-chip Raman microscopy[95]. Efficient on-chip implementations typically require advanced fabrication techniques, which are expected to be further improved in the future. Specifically, recent advances in optical metasurfaces[96,97] might bring to new efficient on-chip implementations of various label-free imaging techniques.

Given that each label-free imaging technique might be based on a different overall contrast mechanism, as well as provide different quantitative values, multimodal imaging methods are beneficial. One can think of two end-member strategies for this combination of different label-free imaging methods. On one end, imaging modalities with similar acquisition speeds and resolutions could be combined, all of which are efficiently excited by the same laser source and can be detected in parallel[98].

Specifically, SLAM[39] offers precise spatiotemporal correlation of 2PF and 3PF, SHG, THG and even CARS through single-shot excitation of ultrafast pulses from a supercontinuum source, followed by fast parallel detection for each of these modalities, as demonstrated in Figs. 3 and 4, presenting convincing potential for label-free cancer identification, even in vivo. A future focus in this field is investigating the dynamic living tumour–tissue microenvironment without perturbative dyes or stains, as well as being able to do this in real time at point-of-care sites. For example, the potential for label-free cancer diagnosis via label-free imaging of extracellular vesicles in situ with single-vesicle spatiotemporal resolution has been demonstrated in tissue, serum and urine[56,99]. In contrast, all other current methods require extraction of tissue and isolation of vesicles, while losing the spatiotemporal context of these vesicles and their signatures of cancer. The fact that there is no drug (exogenous marker) involved enables rapid translation to clinical studies, trials and eventually use.

More examples for applications of interest for label-free multimodal imaging include characterizing the metabolic dynamics in neurons and astrocytes and label-free detection of neural activity and connectivity in neuronal cultures via rapid FLIM, OCT and other multimodal techniques[100,101], label-free detection and characterization of amyloid-beta plaques in brain-tissue slices via 3PF and THG[102], and tumour-boundary label-free detection via combined SHG, 3PF

and CARS during surgery. For the latter application a major step forwards would be the implementation of spectroscopic-guided ablation combined with an endoscope[103] in a seek-and-treat manner, allowing real-time monitoring of the features of the ablated tissue. Co-registered multimodal image datasets are ideally suited to high-dimensional AI analysis and for correlating between the various contrast mechanisms and the underlying physics[104]. On the other end, imaging modalities of different imaging speeds and tissue penetration depths could be synergistically combined, so that a fast but chemically less-specific method provides an overview on the tissue volume, while a slower, molecule-specific second method is used to classify tissues detected by the faster modality in suspicious areas. One such approach would be to combine OCT or FLIM with Raman microscopy[21,22,105].

The development of these label-free imaging modalities also offers the advantage of longitudinal imaging, such as fast imaging capturing dynamics over time periods of seconds, or longer time-lapse imaging over periods of minutes to hours. Without the concerns of dye photobleaching, potential toxicity and perturbative changes to the biological processes under investigation, these label-free imaging modalities can be used to explore various time-dependent cellular activities and biological functions, such as rapid sperm dynamics[9] and neural activity[100], cell-death processes[101], and intercellular communications via extracellular vesicles and organelle trafficking[56]. There are opportunities for using these unique dynamic nonperturbing features of label-free biomedical imaging for discovering new biological principles, as well as new biomarkers indicative of disease.

Finally, the measurability of new characteristics of the light field, beyond the intensity distribution, opens up new conceptual and technological possibilities for biomedical research. New light sources generating noise-free quantum states might yield future label-free imaging methods that rely on the correlations between photons and detector systems[106,107].

To conclude, against label-based imaging, label-free imaging wins when studying live biological processes in cells and tissues, where exogenous markers perturb the biology studied—especially in longitudinal studies or monitoring. In the near future, label-free imaging will clearly win in in vivo applications in general, and in intraoperative diagnosis in particular, where using exogenous markers is both time consuming and requires regulations and safety approvals that may take years to obtain. We thus expect that, despite the challenges in the field that are yet to be addressed, label-free imaging will become more and more attractive and popular for both biological assays and clinical applications.

References

1. Zernike, F. How I discovered phase contrast. *Science* **121**, 345–349 (1955).
2. Lang, W. Nomarski differential interference-contrast microscopy. *Zeiss Inf.* **70**, 114–120 (1968).
3. Marquet, P. et al. Digital holographic microscopy: a noninvasive contrast imaging technique allowing quantitative visualization of living cells with subwavelength axial accuracy. *Opt. Lett.* **30**, 468–470 (2005).
4. Girshovitz, P. & Shaked, N. T. Generalized cell morphological parameters based on interferometric phase microscopy and their application to cell life cycle characterization. *Biomed. Opt. Express* **3**, 1757–1773 (2012).
5. Park, Y. K., Depeursinge, C. & Popescu, G. Quantitative phase imaging in biomedicine. *Nat. Photon.* **12**, 578–589 (2018).
6. Haifler, M. et al. Interferometric phase microscopy for label-free morphological evaluation of sperm cells. *Fertil. Steril.* **104**, 43–47 (2015).
7. Choi, W. et al. Tomographic phase microscopy. *Nat. Methods* **4**, 717–719 (2007).
8. Jin, D., Zhou, R., Yaqoob, Z. & So, P. T. C. Tomographic phase microscopy: principles and applications in bioimaging. *J. Opt. Soc. Am. B* **34**, B64–B77 (2017).
9. Dardikman-Yoffe, G., Mirsky, S. K., Barnea, I. & Shaked, N. T. High-resolution 4-D acquisition of freely swimming human sperm cells without staining. *Sci. Adv.* **6**, eaay7619 (2020).
10. Oldenbourg, R. *Imaging: A Laboratory Manual* (ed. Yuste, R.) (CSHL, 2011).
11. Oldenbourg, R. Polarized light microscopy of spindles. *Methods Cell. Biol.* **61**, 175–208 (1998).
12. Koike-Tani, M., Tani, T., Mehta, S. B., Verma, A. & Oldenbourg, R. Polarized light microscopy in reproductive and developmental biology. *Mol. Reprod. Dev.* **82**, 548–562 (2013).
13. Drexler, W. & Fujimoto J. G. *Optical Coherence Tomography: Technology and Applications* (Springer, 2008).
14. Leitgeb, R., Hitzenberger, C. K. & Fercher, A. F. Performance of Fourier domain vs. time domain optical coherence tomography. *Opt. Express* **11**, 889–894 (2003).
15. Hillmann, D. et al. Aberration-free volumetric high-speed imaging of in vivo retina. *Sci. Rep.* **6**, 35209 (2016).
16. Duker, J. S., Waheed, N. K. & Goldman, D. *Handbook of Retinal OCT: Optical Coherence Tomography* (Elsevier, 2013).
17. Shemonski, N. D. et al. Computational high-resolution optical imaging of the living human retina. *Nat. Photon.* **9**, 440–443 (2015).
18. Tearney, G. J. et al. Three-dimensional coronary artery microscopy by intracoronary optical frequency domain imaging. *JACC Cardiovasc. Imag.* **1**, 752–761 (2008).
19. Raffel, O. C., Akasaka, T. & Jang, I.-K. Cardiac optical coherence tomography. *Heart* **94**, 1200–1210 (2008).
20. Tearney, G. J. et al. In vivo endoscopic optical biopsy with optical coherence tomography. *Science* **276**, 2037–2039 (1997).
21. Nolan, R. M. et al. Intraoperative optical coherence tomography for assessing human lymph nodes for metastatic cancer. *BMC Cancer* **16**, 144 (2016).
22. Erickson-Bhatt, S. J. et al. Real-time imaging of the resection bed using a handheld probe to reduce incidence of microscopic positive margins in cancer surgery. *Cancer Res.* **75**, 3706–3712 (2015).
23. Poneros, J. M. & Nishioka, N. S. Diagnosis of Barrett's esophagus using optical coherence tomography. *Gastrointest. Endosc. Clin. N. Am.* **13**, 309–323 (2013).
24. Dong, J. et al. Feasibility and safety of tethered capsule endomicroscopy in patients with Barrett's esophagus in a multi-center study. *Clin. Gastroenterol. Hepatol.* **20**, 756–765 (2022).
25. Sattler, E., Kästle, R. & Welzel, J. Optical coherence tomography in dermatology. *J. Biomed. Opt.* **18**, 061224 (2013).
26. Gambichler, T. et al. Applications of optical coherence tomography in dermatology. *J. Dermatol. Sci.* **40**, 85–94 (2005).
27. Byers, R. A. et al. Sub-clinical assessment of atopic dermatitis severity using angiographic optical coherence tomography. *Biomed. Opt. Express* **9**, 2001–2017 (2018).
28. Larina, I. V. et al. Live imaging of blood flow in mammalian embryos using Doppler swept-source optical coherence tomography. *J. Biomed. Opt.* **13**, 060506 (2008).
29. Singh, M. et al. Applicability, usability, and limitations of murine embryonic imaging with optical coherence tomography and optical projection tomography. *Biomed. Opt. Express* **7**, 2295–2310 (2016).
30. Park, S. et al. Quantitative evaluation of the dynamic activity of HeLa cells in different viability states using dynamic full-field optical coherence microscopy. *Biomed. Opt. Express* **12**, 6431–6441 (2021).
31. Mecê, P., Scholler, J., Groux, K. & Boccara, C. High-resolution in-vivo human retinal imaging using full-field OCT with optical stabilization of axial motion. *Biomed. Opt. Express* **11**, 492–504 (2020).
32. Ralston, T. S., Marks, D. L., Carney, P. S. & Boppart, S. A. Interferometric synthetic aperture microscopy. *Nat. Phys.* **3**, 129–134 (2007).

33. Mohler, W., Millard, A. C. & Campagnola, P. J. Second harmonic generation imaging of endogenous structural proteins. *Methods* **29**, 97–109 (2003).
34. Conklin, M. W. et al. Aligned collagen is a prognostic signature for survival in human breast carcinoma. *Am. J. Pathol.* **178**, 1221–1232 (2011).
35. Quinn, K. P. et al. Optical metrics of the extracellular matrix predict compositional and mechanical changes after myocardial infarction. *Sci. Rep.* **6**, 35823 (2016).
36. Chu, S.-W., Tai, S.-P., Ho, C.-L., Lin, C.-H. & Sun, C.-K. High-resolution simultaneous three-photon fluorescence and third-harmonic-generation microscopy. *Microsc. Res. Techn.* **66**, 193–197 (2005).
37. Tsai, M.-R., Chen, S.-Y., Shieh, D.-B., Lou, P.-J. & Sun, C.-K. In vivo optical virtual biopsy of human oral mucosa with harmonic generation microscopy. *Biomed. Opt. Express* **2**, 2317–2328 (2011).
38. Walsh, A. J. et al. Classification of T-cell activation via autofluorescence lifetime imaging. *Nat. Biomed. Eng.* **5**, 77–88 (2020).
39. You, S. et al. Intravital imaging by simultaneous label-free autofluorescence-multiharmonic microscopy. *Nat. Commun.* **9**, 2125 (2018).
40. Skala, M. C. et al. In vivo multiphoton microscopy of NADH and FAD redox states, fluorescence lifetimes, and cellular morphology in precancerous epithelia. *Proc. Natl Acad. Sci. USA* **104**, 19494–19499 (2007).
41. Liu, Z., Meng, J., Quinn, K. P. & Georgakoudi, I. Tissue imaging and quantification relying on endogenous contrast. *Adv. Exp. Med. Biol.* **3233**, 257–288 (2021).
42. Becker, W., Bergmann, A. & Biskup, C. Multispectral fluorescence lifetime imaging by TCSPC. *Microsc. Res. Techn.* **70**, 403–409 (2007).
43. Sorrells, J. E. et al. Computational photon counting using multi-threshold peak detection for fast fluorescence lifetime imaging microscopy. *ACS Photon.* **9**, 2748–2755 (2022).
44. Bower, A. J. et al. Label-free in vivo cellular-level detection and imaging of apoptosis. *J. Biophoton.* **10**, 143–150 (2017).
45. Li, Q. et al. Review of spectral imaging technology in biomedical engineering: achievements and challenges. *J. Biomed. Optics* **18**, 100901 (2013).
46. Kole, M. R., Reddy, R. K., Schulmerich, M. V., Gelber, M. K. & Bhargava, R. Discrete frequency infrared microspectroscopy and imaging with a tunable quantum cascade laser. *Anal. Chem.* **84**, 10366–10372 (2012).
47. Pilling, M. J., Henderson, A. & Gardner, P. Quantum cascade laser spectral histopathology: breast cancer diagnostics using high throughput chemical imaging. *Anal. Chem.* **89**, 7348–7355 (2017).
48. Kuepper, C. et al. Quantum cascade laser-based infrared microscopy for label-free and automated cancer classification in tissue sections. *Sci. Rep.* **8**, 7717 (2018).
49. Zhang, D. et al. Depth-resolved mid-infrared photothermal imaging of living cells and organisms with submicrometer spatial resolution. *Sci. Adv.* **2**, e1600521 (2016).
50. Nedosekin, D. A., Galanzha, E. I., Dervishi, E., Biris, A. S. & Zharov, V. P. Super-resolution nonlinear photothermal microscopy. *Small* **10**, 135–142 (2014).
51. Brauchle, E. & Schenke-Layland, K. Raman spectroscopy in biomedicine – non-invasive in vitro analysis of cells and extracellular matrix components in tissues. *Biotechnol. J.* **8**, 288–297 (2013).
52. Krafft, C. et al. Label-free molecular imaging of biological cells and tissues by linear and nonlinear Raman spectroscopic approaches. *Angew. Chem. Int. Ed.* **56**, 4392–4431 (2017).
53. Lee, K. S. et al. Raman microspectroscopy for microbiology. *Nat. Rev. Methods Primers* **1**, 80 (2021).
54. Matanfack, G. A., Rüger, J., Stiebing, C., Schmitt, M. & Popp, J. Imaging the invisible—bioorthogonal Raman probes for imaging of cells and tissues. *J. Biophoton.* **13**, e202000129 (2020).
55. Zumbusch, A., Holtom, G. R. & Xie, X. S. Three-dimensional vibrational imaging by coherent anti-Stokes Raman scattering. *Phys. Rev. Lett.* **82**, 4142–4145 (1999).
56. Tu, H. et al. Concurrence of extracellular vesicle enrichment and metabolic switch visualized label-free in the tumor microenvironment. *Sci. Adv.* **3**, e1600675 (2017).
57. Liu, Y. et al. Label-free molecular profiling for identification of biomarkers in carcinogenesis using multimodal multiphoton imaging. *Quant. Imag. Med. Surg.* **9**, 742–756 (2019).
58. Freudiger, C. W. et al. Label-free biomedical imaging with high sensitivity by stimulated Raman scattering microscopy. *Science* **322**, 1857–1861 (2008).
59. Cheng, J.-X., Min, W., Ozeki, Y. & Polli, D. *Stimulated Raman Scattering Microscopy: Techniques and Applications* (Elsevier, 2022).
60. Wang, L. V. & Hu, S. Photoacoustic tomography: in vivo imaging from organelles to organs. *Science* **335**, 1458–1462 (2012).
61. Wang, X. D. et al. Noninvasive laser-induced photoacoustic tomography for structural and functional in vivo imaging of the brain. *Nat. Biotechnol.* **21**, 803–806 (2003).
62. Siphanto, R. I. et al. Serial noninvasive photoacoustic imaging of neovascularization in tumor angiogenesis. *Opt. Express* **13**, 89–95 (2005).
63. Laufer, J., Delpy, D., Elwell, C. & Beard, P. Quantitative spatially resolved measurement of tissue chromophore concentrations using photoacoustic spectroscopy: application to the measurement of blood oxygenation and haemoglobin concentration. *Phys. Med. Biol.* **52**, 141–168 (2007).
64. Zhang, H. F., Maslov, K., Stoica, G. & Wang, L. V. Functional photoacoustic microscopy for high-resolution and noninvasive in vivo imaging. *Nat. Biotechnol.* **24**, 848–851 (2006).
65. Xu, M. H. & Wang, L. V. Universal back-projection algorithm for photoacoustic computed tomography. *Phys. Rev. E* **71**, 016706 (2005).
66. Nagae, K. et al. Real-time 3D photoacoustic visualization system with a wide field of view for imaging human limbs. *F1000Research* **7**, 1813 (2018).
67. Lin, L. et al. Single-breath-hold photoacoustic computed tomography of the breast. *Nat. Commun.* **9**, 2352 (2018).
68. Dantuma, M. et al. Fully three-dimensional sound speed-corrected multi-wavelength photoacoustic breast tomography. Preprint at https://arxiv.org/abs/2308.06754 (2023).
69. Na, S. et al. Massively parallel functional photoacoustic computed tomography of the human brain. *Nat. Biomed. Eng.* **6**, 584–592 (2022).
70. Wong, T. T. et al. Fast label-free multilayered histology-like imaging of human breast cancer by photoacoustic microscopy. *Sci. Adv.* **3**, e1602168 (2017).
71. Li, L. et al. Single-impulse panoramic photoacoustic computed tomography of small-animal whole-body dynamics at high spatiotemporal resolution. *Nat. Biomed. Eng.* **1**, 0071 (2017).
72. Sun, Y. et al. Detection of weak near-infrared optical imaging signals under ambient light by optical parametric amplification. *Opt. Lett.* **44**, 4391–4394 (2019).
73. Schürmann, M., Scholze, J., Müller, P., Guck, J. & Chan, C. J. Cell nuclei have lower refractive index and mass density than cytoplasm. *J. Biophoton.* **9**, 1068–1076 (2016).
74. Rivenson, Y. et al. Virtual histological staining of unlabelled tissue-autofluorescence images via deep learning. *Nat. Biomed. Eng.* **3**, 466–477 (2019).
75. Nygate, Y. N. et al. Holographic virtual staining of individual biological cells. *Proc. Natl Acad. Sci. USA* **117**, 9223–9231 (2020).
76. Kandel, M. E. et al. Phase imaging with computational specificity (PICS) for measuring dry mass changes in sub-cellular compartments. *Nat. Commun.* **11**, 6256 (2020).
77. You, S., Chaney, E. J., Tu, H., Sinha, S. & Boppart, S. A. Label-free deep profiling of the tumor microenvironment. *Cancer Res.* **81**, 2534–2544 (2021).

78. Krafft, C. & Popp, J. Opportunities of optical and spectral technologies in intraoperative histopathology. *Optica* **10**, 214–231 (2023).
79. Pradhan, P. et al. Computational tissue staining of non-linear multimodal imaging using supervised and unsupervised deep learning. *Biomed. Opt. Express* **12**, 2280–2298 (2021).
80. You, S. et al. Real-time intraoperative diagnosis by deep neural network driven multiphoton virtual histology. *Precis. Oncol.* **3**, 33 (2019).
81. Hell, S. W. et al. The 2015 super-resolution microscopy roadmap. *J. Phys. D* **48**, 443001 (2015).
82. Cotte, Y. et al. Marker-free phase nanoscopy. *Nat. Photon.* **7**, 113–117 (2013).
83. Bi, Y. et al. Near-resonance enhanced label-free stimulated Raman scattering microscopy with spatial resolution near 130 nm. *Light Sci. Appl.* **7**, 81 (2018).
84. Gong, L., Zheng, W., Ma, Y. & Huang, Z. Higher-order coherent anti-Stokes Raman scattering microscopy realizes label-free super-resolution vibrational imaging. *Nat. Photon.* **14**, 115–122 (2020).
85. Danielli, A. et al. Label-free photoacoustic nanoscopy. *J. Biomed. Opt.* **19**, 086006 (2014).
86. Fu, P. et al. Super-resolution imaging of non-fluorescent molecules by photothermal relaxation localization microscopy. *Nat. Photon.* **17**, 330–337 (2023).
87. Lindfors, K., Kalkbrenner, T., Stoller, P. & Sandoghdar, V. Detection and spectroscopy of gold nanoparticles using supercontinuum white light confocal microscopy. *Phys. Rev. Lett.* **93**, 037401 (2004).
88. Foley, E. D. B., Kushwah, M. S., Young, G. & Kukura, P. Mass photometry enables label-free tracking and mass measurement of single proteins on lipid bilayers. *Nat. Methods* **18**, 1247–1252 (2021).
89. Heermann, T., Steiert, F., Ramm, B., Hundt, N. & Schwille, P. Mass-sensitive particle tracking to elucidate the membrane-associated MinDE reaction cycle. *Nat. Methods* **18**, 1239–1246 (2021).
90. Sun, Y. et al. Intraoperative visualization of the tumor microenvironment and quantification of extracellular vesicles by label-free nonlinear imaging. *Sci. Adv.* **4**, eaau5603 (2018).
91. Monroy, G. M., Won, J., Spillman, D. R., Dsouza, R. & Boppart, S. A. Clinical translation of handheld optical coherence tomography: practical considerations and recent advances. *J. Biomed. Optics* **22**, 121715 (2017).
92. Jermyn, M. et al. Intraoperative brain cancer detection with Raman spectroscopy in humans. *Sci. Transl. Med.* **7**, 274ra19 (2015).
93. Pshenay-Severin, E. et al. Multimodal nonlinear endomicroscopic imaging probe using a double-core double-clad fiber and focus-combining micro-optical concept. *Light Sci. Appl.* **10**, 207 (2021).
94. Rank, E. A. et al. Toward optical coherence tomography on a chip: in vivo three-dimensional human retinal imaging using photonic integrated circuit-based arrayed waveguide gratings. *Light Sci. Appl.* **10**, 6 (2021).
95. Wuytens, P. C., Skirtach, A. G. & Baets, R. On-chip surface-enhanced Raman spectroscopy using nanosphere-lithography patterned antennas on silicon nitride waveguides. *Opt. Express* **25**, 12926–12934 (2017).
96. Yu, N. & Capasso, F. Flat optics with designer metasurfaces. *Nat. Mater.* **13**, 139–150 (2014).
97. Neshev, D. & Aharonovich, I. Optical metasurfaces: new generation building blocks for multi-functional optics. *Light Sci. Appl.* **7**, 58 (2018).
98. Meyer, T. et al. A compact microscope setup for multimodal nonlinear imaging in clinics and its application to disease diagnostics. *Analyst* **138**, 4048–4057 (2013).
99. You, S. et al. Label-free visualization and characterization of extracellular vesicles in breast cancer. *Proc. Natl Acad. Sci. USA* **116**, 24012–24018 (2019).
100. Iyer, R. R. et al. Ultra-parallel label-free optophysiology of neural activity. *iScience* **25**, 104307 (2022).
101. Bower, A. J. et al. High-speed imaging of transient metabolic dynamics using two-photon fluorescence lifetime imaging microscopy. *Optica* **5**, 1290–1296 (2018).
102. Tehrani, K.F., Park, J., Renteria, C. & Boppart, S.A. Label-free identification of Alzheimer's disease plaques using multiple co-registered nonlinear optical biomarkers. In *Clinical and Translational Neurophotonics, SPIE Photonics West BiOS* 12364-2 (SPIE, 2023).
103. Lai, C. et al. Design and test of a rigid endomicroscopic system for multimodal imaging and femtosecond laser ablation. *J. Biomed. Optics* https://doi.org/10.1117/1.JBO.28.6.066004 (2023).
104. Chernavskaia, O. et al. Beyond endoscopic assessment in inflammatory bowel disease: real-time histology of disease activity by non-linear multimodal imaging. *Sci. Rep.* **6**, 29239 (2016).
105. Fitzgerald, S. et al. Multimodal Raman spectroscopy and optical coherence tomography for biomedical analysis. *J. Biophoton.* https://doi.org/10.1002/jbio.202200231 (2023).
106. Kalashnikov, D. A., Paterova, A. V., Kulik, S. P. & Krivitsky, L. A. Infrared spectroscopy with visible light. *Nat. Photon.* **10**, 98–101 (2016).
107. Barreto Lemos, G. et al. Quantum imaging with undetected photons. *Nature* **512**, 409–412 (2014).

Acknowledgements

We acknowledge the support of the following grants: Horizon2020 ERC grant (678316) (PI: N.T.S.). NIH Center for Label-free Imaging and Multiscale Biophotonics (CLIMB) at the University of Illinois Urbana-Champaign (http://climb.beckman.illinois.edu) P41 EB031772 and NIH grant numbers R01 CA241618 and R01 CA213149 (PI: S.A.B.). NIH grant numbers R01 NS102213, U01 EB029823 (BRAIN Initiative), R35 CA220436 (Outstanding Investigator Award), and R01 EB028277 (PI: L.V.W.).

Competing interests

The authors declare no competing interests.

Additional information

Correspondence and requests for materials should be addressed to Natan T. Shaked.

Peer review information *Nature Photonics* thanks Paul Campagnola, Ping Wang and the other, anonymous, reviewer(s) for their contribution to the peer review of this work.